forests

MDPI

Article

Sustainable Supercapacitor Electrode Based on Activated Biochar Derived from Preserved Wood Waste

Meiling Huang [1], Boren Dai [1], Jiangtao Shi [1,2,*], Jiayao Li [1] and Changlei Xia [1,2]

[1] College of Materials Science and Engineering, Nanjing Forestry University, Nanjing 210037, China
[2] Co-Innovation Center of Efficient Processing and Utilization of Forest Resources, Nanjing Forestry University, Nanjing 210037, China
* Correspondence: shijt@njfu.edu.cn

Abstract: Due to the inherent metals (Cu, As and Cr) in preserved wood waste (CCA-treated wood waste) that pose a risk to both the environment and human health, it is crucial to dispose of CCA-treated wood properly. Carbon materials have received widespread attention for their high porosity, renewability and simplicity of fabrication. This work presents a simple and effective process for producing carbon materials from leftover CCA-treated wood (chromated copper arsenate). Utilizing CCA-treated wood derived carbon (CCA-BC) and activating it with KOH (CCA-AC), electrode materials for supercapacitor applications were created and its electrochemical characteristics were investigated. The resulting material combines the conductivity of the metal in preserved wood with the good porosity provided by carbon materials. Compared with common wood biomass, carbon (W-BC) and common wood activated carbon (W-AC), CCA-BC and CCA-AC have better electrochemical properties. After being pyrolyzed at 600 °C for two hours, CCA-AC performed optimally electrochemically in 1 M Na_2SO_4 electrolyte, demonstrating a 72% capacity retention rate after 2000 charge and discharge cycles and a specific capacity of 76.7 F/g. This study provides a novel approach for the manufacture of supercapacitor electrodes, which also allows preserved wood waste an environmentally nondestructive form of elimination.

Keywords: CCA-treated wood; activated carbon electrode; electrochemical properties

Citation: Huang, M.; Dai, B.; Shi, J.; Li, J.; Xia, C. Sustainable Supercapacitor Electrode Based on Activated Biochar Derived from Preserved Wood Waste. *Forests* **2024**, *15*, 177. https://doi.org/10.3390/f15010177

Academic Editors: Irena Bates, Ivana Plazonić, Mia Kurek and Nikola Španić

Received: 13 December 2023
Revised: 9 January 2024
Accepted: 12 January 2024
Published: 15 January 2024

1. Introduction

Wood preservatives are used to prevent wood from biodeterioration. Waterborne chromated copper arsenic (CCA) is a representative preservative that has been widely used in wood structure building and outdoor landscaping for over 100 years [1,2]. Over the next fifty years, large amounts of wood waste will enter the wood waste stream due to the wood's increased service life. Because the ingredients of CCA preservation are arsenic pentoxide (As_2O_5, 34%), copper oxide (CuO) and chromium trioxide (CrO_3, 47.5%), preserved wood waste treated by CCA can result in an excessive release of high concentrations of toxic heavy metal ions into the environment, which can pose great threat to human and ecological health [3–6]. Although many countries have prohibited the production and utilization of CCA-treated wood [7,8], according to reports, the soils next to CCA-wood have concentrations as high as 110 mg/kg [7], which is higher than the USEPA's ecological soil screening limit [8]. It is urgently necessary to figure out how to appropriately post-treat the abandoned preserved wood.

Although many approaches have been investigated to reduce the adverse effects of CCA-treated wood, recycling still attracts increasing attention. The upcycling of solid waste is environmentally friendly, cost-effective and low energy, which meets the requirements of sustainable development [9]. Various means have been used to reuse the waste of CCA-treated wood, such as wood composites [10,11], copper-doped carbon nanodots [12] and so on. However, there are few reports on upcycling CCA-treated wood waste at a high added value. Wood, consisting of cellulose, hemicellulose and lignin, is a good carbon sink

material. CCA-treated wood waste has been directly thermally transformed into biochar, which has good dielectric properties [13,14].

Energy is one of the most important issues of the twenty-first century. Energy efficiency is highly desired due to the quick depletion of fossil resources and the deteriorating environmental contamination brought on by widespread usage of fossil fuels [15,16]. Under these conditions, supercapacitors have drawn a lot of research interest due to their rapid charging times, great power density and incredibly extended cycle life [17]. Generally, supercapacitors can be broadly classified into three classical categories: hybrid, pseudo and electrical double-layer (EDLC) supercapacitors. Carbon materials possess the merits of excellent electrical conductivity, rapid electron transport velocity, substantial and adjustable porosity and extensive electrolyte channels, as well as remarkable thermal stability, which make them promising as EDLC supercapacitor candidates [18]. The combination of metals and carbon have been widely reported in the field of supercapacitors [19–21]. Many studies have reported that when metal compounds were hybridized with carbon, hybrid supercapacitors with high energy storage density could be obtained, in which carbon materials primarily stored charge by an EDLC mechanism, possessing high specific surface area, fast electron transport velocity and great electrical conductivity, while metal compounds could store charge through a pseudocapacitance mechanism [22,23]. Reducing the electric double layer that forms on the electrode surface as a result of the irreversible adsorption of ions in the electrolyte can lower the capacitance of the carbon electrode [24]. Making composite materials with higher stability capacitance—that is, combining bilayer capacitance with REDOX (pseudocapacitance)—could be one way to get around these limitations. But as a double-layer electrode, the poor capacitance of carbon materials can be fixed by adding metal. Because it can successfully transmit ions and electrons via the electrode, it can extend the life of the charge and discharge cycle in addition to improving power and energy density [25]. Due to its low cost, wood-derived activated biochar has garnered special attention recently as a potential supercapacitor electrode material with tunable pore structure, multiple functional groups and environmental friendliness. Therefore, CCA-treated wood can be potentially fabricated into EDLC and/or hybrid supercapacitors through pyrolysis with activating agents. During this process the impregnated metal ions could be converted in situ into corresponding metal compounds and anchored within the biochar skeleton.

In this study, activated biochar was prepared from CCA-treated wood waste by direct pyrolysis combined with chemical activation, in which KOH was introduced as the activation agent. The prepared biochar samples were used afterwards as the electrode of a supercapacitor. In order to find out how the calcination temperature affected the functional group and electrochemical characteristics of the BC and AC electrodes, an assessment of the associated characterization and performance measurements was also carried out concurrently. The effects of impregnation with CCA preservative on the electrochemical characteristics of the biochar electrodes were also compared.

2. Materials and Methods

2.1. Preparation of CCA-Treated Wood Waste Biochar (CCA-BC) and Its Activation by KOH (CCA-AC)

You can find a list of the raw materials and chemicals utilized in this investigation in Text S1 of the Supplementary Materials. The CCA-treated wood was first ground into a powder, put through a screen with an 80–100 mesh size and then roasted for 24 h at 60 °C in an oven to dry it out before processing. Then, in a tube furnace with a N_2 environment, ground wood powder was heated to a predetermined temperature at a rate of 5 °C/min and pyrolyzed at the corresponding temperature for a given time (2 h). Upon reaching room temperature, the resulting CCA-BC-x was produced, where x represents the temperature at which pyrolyzing occurred (400, 500 or 600 °C). Afterwards, CCA-BC-x (1.0 g) and potassium hydroxide (KOH, 3.0 g) were added into 20 mL of distilled water, and stirred for 4 h. Afterwards, the solution was put into an oven and dried at 60 °C for 24 h. The dried mixture was then pyrolyzed at 400, 500 and 600 °C for another 2 h for activation. Upon

achieving a neutral pH through washing with distilled water and alcohol, the resulting activated biochar was dried for 24 h at 60 °C. The resulting CCA-AC-x was obtained. For comparison, Douglas fir pyrolyzed biochar samples (W-BC) and activated biochar samples (W-AC) without CCA treatment were also prepared following similar routes.

2.2. Characterization and Analytical Methods

The thermogravimetric analysis (TGA) was conducted using NETZSCH-Gerätebau GmbH-TG209F3 (the maximum temperature was set at 900 °C and the heating rate was 5 °C/min). FEI Quanta 200 was used to perform scanning electron microscopy (SEM) at a working distance of 15–20 mm with an electron beam intensity of 20 kV. A Cu-Kα radiation source-equipped Rigaku Smartlab XRD apparatus was used to study the X-ray diffraction (XRD) patterns. The AXIS UltraDLD spectrometer was used to perform X-ray photoelectron spectroscopy (XPS). An Ar laser (532 nm, 180 mW) was used as the excitation light source, and the DXR532 Raman spectrometer was used to record the Raman spectra. Measurements of the nitrogen adsorption–desorption isotherms at 77 K were made with a Micromeritics ASAP 2020 HD88. Both total pore volume and BET surface area and pore size were within 5% error.

2.3. Electrochemical Test

To investigate the electrochemical characteristics of the produced biochar samples, using as synthesized biochar as the working electrode and a platinum sheet as the counter electrode, a three electrode system was put together; Ag/AgCl served as the reference electrode (RE) and Na_2SO_4 (1 M) served as the electrolyte. The working electrode was prepared by slurry coating. To be more precise, a slurry (~5 mg) of biochar, acetylene black and polyvinyl difluoride (PVDF) with a weight ratio of 8/1/1 was made using N-methyl pyrrolidinone (NMP) as the solvent. After that, the combination slurry was applied to a 1.5×1.0 cm^2 nickel foam slice. The coated sections were squeezed at a pressure of roughly 10 MPa after being dried for 24 h at 60 °C in a vacuum drying oven. The galvanostatic charge–discharge (GCD), electrochemical impedance spectra (EIS) and cyclic voltammetry (CV) measurements were performed using a CHI660E electrochemical workstation.

3. Results and Discussion

3.1. Thermo Gravimetric Analysis of Raw Wood Materials

In order to obtain information about the change in sample mass and mass change rate as a function of the process temperature, thermogravimetric analysis of the original wood samples (common Douglas fir and preserved wood) in air and N_2, respectively. The TGA curves of the raw materials pyrolyzed under air atmosphere are shown in Figure 1a, which shows that the final residue of preserved wood is higher than that of common wood, it is the metal compounds in the preserved wood that lead to this result, and the total amount of metal compounds remaining is about 4.5 wt%. On the other hand, the TGA curves demonstrated the stages of mass loss during the complete charring process of the two wood materials, and it can be clearly seen that under a nitrogen atmosphere (Figure 1b), the mass of the two samples changed very little between 50–200 °C, indicating that the samples had a low water content, and the mass decreased sharply at the 200–350 °C stage, which was due to the pyrolysis of hemicellulose and cellulose. The lower structural stability of hemicellulose and cellulose leads to the earlier completion of pyrolysis of these two components. Between 400–900 °C, the mass loss rate of the sample tends to stabilize, which is due to the fact that after the completion of hemicellulose and cellulose pyrolysis, the remaining lignin pyrolysis temperature in the sample is at 900 °C or above.

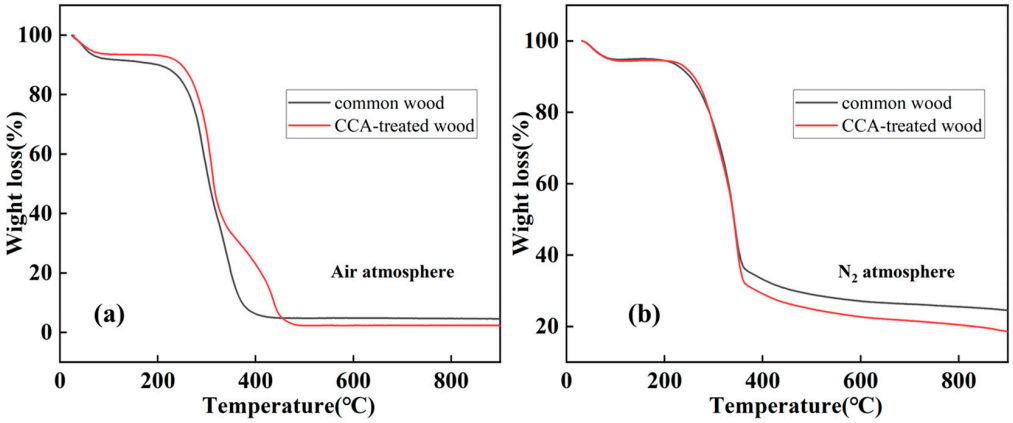

Figure 1. TGA curves of common wood and CCA-treated wood under (**a**) air and (**b**) N_2 atmosphere.

3.2. Characterizations of the Prepared Biochar Samples

Because of the color of the metallic components in the preservative, the CCA-treated wood had a light green tint prior to pyrolyzing (Figure S1a). Figure S2 demonstrates the EDS analysis of the raw material of preserved wood powder, and the results show that it contains metal elements such as Cu, Cr and As, whereas this was not found in the wood without preservative treatment. Figure 2 shows the SEM images of the CCA-BC-x and CCA-AC-x samples. As shown in the Figure 2a–c, all CCA-BC-x samples exhibited similar appearance, in which curled biochar fibers and sheets derived from pristine wood interlapped tightly. Comparatively, it was clearly seen from Figure 2e–g that due to the activating of the KOH, compared with BC samples, the fiber structures of AC samples were destroyed. All CCA-AC-x samples showed that a sponge-like morphology with abundant pores existed within the skeleton. As the pyrolysis temperature got higher, the pores became more pronounced. A similar phenomenon could be also observed for W-BC-500 and W-AC-500, except that small white particles only appeared in CCA-treated wood derived biochar samples, corresponding to the metal compound particles converted from the CCA preservative. The elements C, O, Cu, Cr and As were all evenly distributed throughout the CCA-AC-600 biochar, according to the X-ray spectroscopy (EDS) elemental mapping images (Figure S3). In addition, in CCA-BC-600, the mass ratio of Cu was 0.66 wt%. The presence of Cu was responsible for the light green color of the preserved wood.

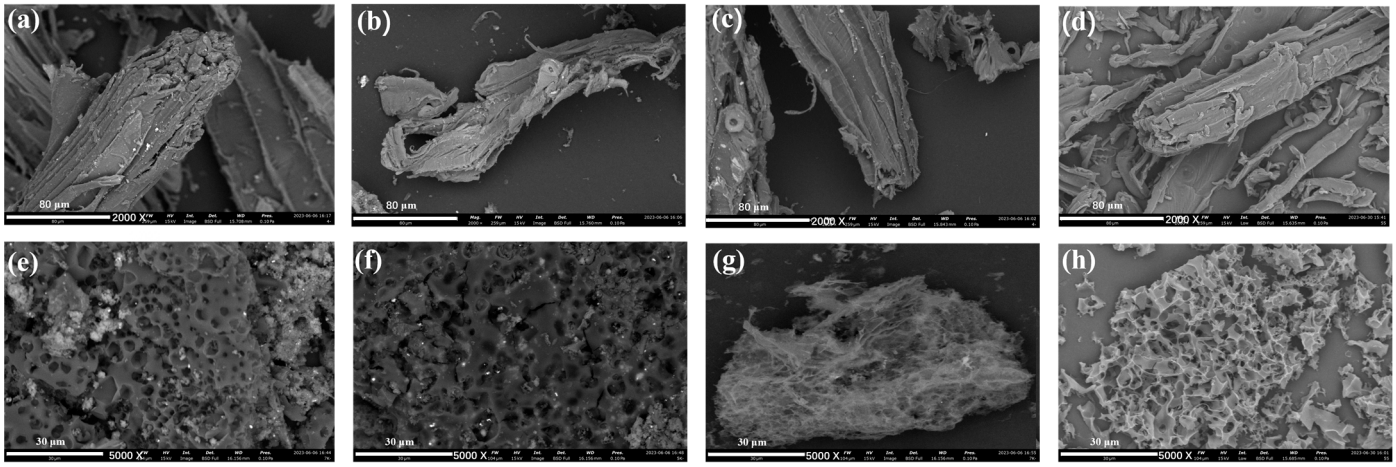

Figure 2. SEM images of (**a**) CCA-BC-400, (**b**) CCA-BC-500, (**c**) CCA-BC-600, (**d**) W-BC-500, (**e**) CCA-AC-400, (**f**) CCA-AC-500, (**g**) CCA-AC-600, (**h**) W-AC-500.

The structure of the generated biochar samples was then examined via XRD; the findings are displayed in Figure 3a,b. It was shown that every sample had a large peak at about 22° that may be attributed to the (002) plane of a graphitic-structured carbonaceous

substance [26]. This indicated that all the wood precursors were converted to carbon with a conjugated structure under pyrolysis treatment. Furthermore, compared to the matching ordinary sample, the graphite peak's strength was lower in the CCA-BC/AC sample. This implies that the biochar's graphite structure's order is weakened by interactions between the metal compounds in CCA and the biochar. It was also revealed that all the patterns contain several sharp peaks. These peaks are related to the conversion of metal compounds from CCA preservative in CCA-treated wood, since these peaks were not observed in the common wood derived biochar samples (Figure S4). The presence of these metal compounds will contribute to the capacitance of the electrode. Through comparing the peaks with the standard spectra, these peaks were identified to be Cu_3As (JCPDS No. 74-1068) and CrO_2 (JCPDS No. 76-1232) [27,28]. In addition, CrO_2 only existed in CCA-AC-x, which indicated that KOH had a certain degree of oxidizing capability. The metal compounds presented in the biochar samples might contribute to the capacitance enhancement capacity of the biochar samples as the electrode.

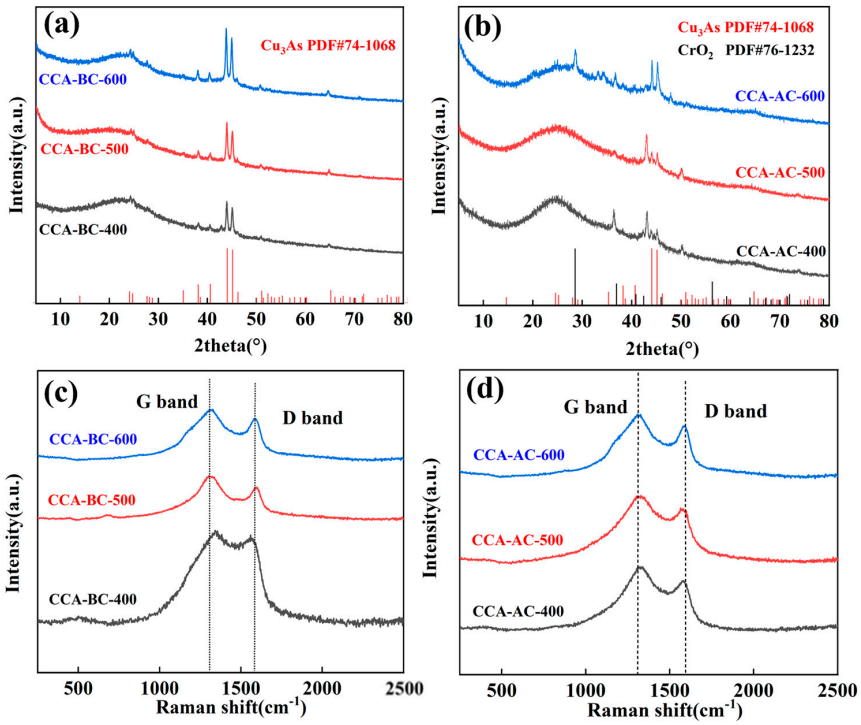

Figure 3. (**a**) XRD spectra of CCA-BC samples and (**b**) CCA-AC samples, (**c**) Raman spectra of CCA-BC samples and (**d**) CCA-AC samples.

Figure 3c,d displays the biochar sample that was created and its Raman spectrum. Both of the typical peaks, at around 1345 cm^{-1} and 1580 cm^{-1}, were clearly visible in every biochar sample. It was evident that every biochar exhibited two characteristic peaks at around 1345 cm^{-1} and 1580 cm^{-1}, respectively. These peaks were attributed to the carbonaceous material's D-band (defective C) and G-band (graphite C) peaks [29,30]. Typically, the intensity ratio (I_D/I_G) between the two bands is utilized to assess the carbon materials' degree of crystallization or defect density [31]. It was revealed that as the pyrolysis temperature rose, the intensity ratio I_D/I_G increased (Table S1). Among them, CCA-AC-600 was as high as 1.46, thus, the condensation process is responsible for the high I_D/I_G values of these carbon samples, which indicated that the biochar samples obtained at higher pyrolysis temperature had more structural defects because, during the pyrolysis process, tiny organic molecules are removed and defective edges are simultaneously formed along the biochar boundary [32]. In addition, all CCA-AC-x had higher I_D/I_G values than their corresponding CCA-BC-x samples. This may be explained by the chemical activation

process's highly porous and disordered structure, which also further damaged the biochar's conjugated structure [33].

Figure 4 shows the XPS spectra of CCA-BC-x samples and CCA-AC-x samples. It was proven that all of the biochar samples included the elements C, O, Cu, Cr and As from the wide-scan XPS spectra displayed in Figure 4a,b, which was consistent with the EDS results. Comparatively, pristine BC and AC derived biochar did not contain metal elements (Figure S5). Based on the elemental proportion analysis (Table S2), it was found that the oxygen proportions of CCA-AC-x samples were all higher than those of their corresponding CCA-BC-x samples, which was because more carbon was oxidized via KOH activation [34,35]. Due to their ability to contribute to the pseudocapacitance of the quinone/hydroquinone redox pair, carbons with oxygen functions may have better electrochemical characteristics than CCA-AC samples [36]. It was further calculated that C/O elemental ratios of CCA-AC samples were all lower than those of their corresponding CCA-BC ones, manifesting that KOH activation brought about more oxygen containing functional groups to the biochar skeleton. It was also found that the C/O ratios of the CCA-BC samples increased with increasing pyrolysis temperature, indicating that during the pyrolysis process, oxygenated groups were progressively eliminated. In contrast, the C/O ratio of the CCA-AC samples dropped as the pyrolysis temperature increased, indicating that a greater temperature promoted the chemical activation of the biochar. Figure 4c,d displays the core-level C1s spectra of the CCA-BC-600 and CCA-AC-600. It was observed that the deconvoluted spectra contain three main peaks located at 284.81 eV, 285.92 eV and 289.41 eV; the peak at 284.81 eV is ascribed to the physically absorbed carbon species or graphitic bonding and the peak at 285.92 eV is assigned to the ether/amide bonding. Additionally, it is possible to relate the peak at 289.41 eV to the carbon structure's ester/carboxylic bond [37,38]. As illustrated, CCA-BC-600 contained a higher proportion of graphitic carbon bonding than CCA-AC-600, suggesting that KOH activation destroyed the graphitic structure in the biochar, which was in accordance with the above discussed results. Additionally, it was discovered that the percentage of graphitic carbon rose for both the CCA-BC and CCA-AC samples as the pyrolysis temperature increased (Figure S6), indicating that greater temperatures might be used to anneal the wood in order to achieve a larger degree of graphitization. Strong interactions between oxygen atoms and metals were also shown in the de-convoluted O1s spectra (Figure S6) in the BC and AC samples [39], and this aligns with the findings of the XRD. Additionally, the hydroxyl group percentages were highest in the activated carbons (CCA-AC-600). This can be explained by the fact that KOH affects activated carbon's properties more noticeably. An ion exchange mechanism changes the -OK groups that are generated on the surface during the KOH activation into -OH groups when the activated carbon is rinsed with water [40].

The structural characteristics of the biochar samples were determined by N_2 adsorption/desorption experiments, and the results are shown in Figure 5 and Table 1. Figure 5a made it evident that CCA-BC-400 had a typical type IV isotherm. The isotherms progressively transitioned to type I isotherms as the pyrolysis temperature rose. The results indicated that micropores dominated CCA-BC-500 and CCA-BC-600. This tendency was also supported by the CCA-BC sample pore size distribution graph (Figure 5b). On the other hand, all CCA-AC samples had H3 type hysteresis loops and a typical type IV isotherm. Figure 5c indicated the mesoporous structures' existence [41], where a small desorption hysteresis and a significant rise at low pressure ($P/P_0 < 0.1$) were also noted. This suggested that the CCA-BC samples had a hierarchical structure in which both micropores and mesopores were presented within the biochar skeleton [42]. The average pore size, total pore volume, and BET specific surface area (SSA) of each examined sample are listed in Table 1. The outcome showed that the samples obtained at higher pyrolysis temperature had larger SSA. Meanwhile, KOH activation enriched porosity of the biochar since the activation process produced abundant gaseous materials including CO, CO_2, H_2O and H_2, which enlarged pores in the internal biochar structure [43]. When the pyrolysis temperature reached 600 °C, the SSA of CCA-AC-600 (885 m^2/g) was almost two times of

that of CCA-BC-600 (445 m^2/g). A similar trend was also observed for total pore volume values. Because the average pore size of the activated materials is larger than 2 nm, the electrolyte ions can more readily enter the pores of the electrode materials. High porosity can also promote the creation of additional electrochemical active centers and electrolyte penetration [44].

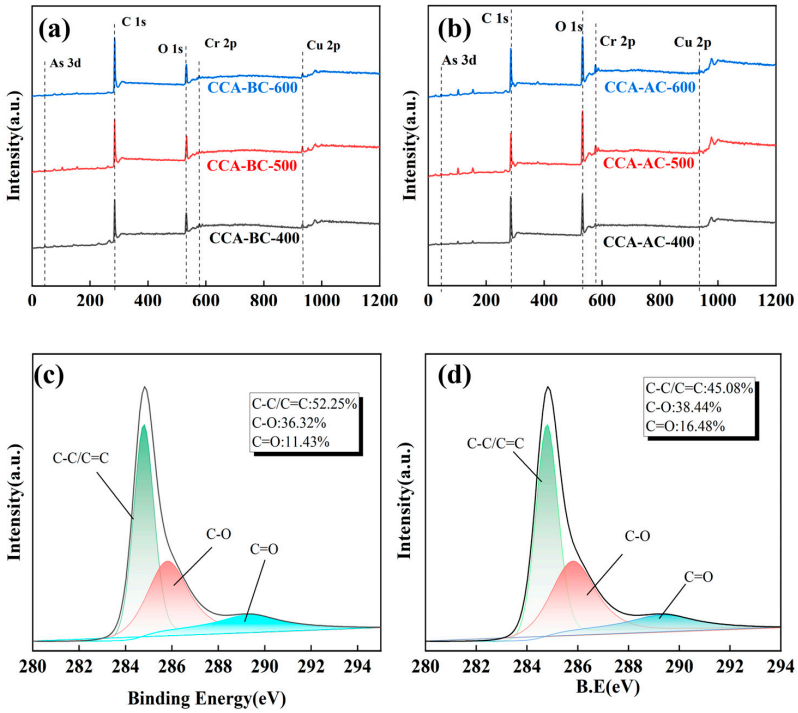

Figure 4. (**a**) Wide-scan XPS spectra of CCA-BC samples and (**b**) CCA-AC samples, (**c**,**d**) C1s XPS spectra of CCA-BC-600 and CCA-AC-600.

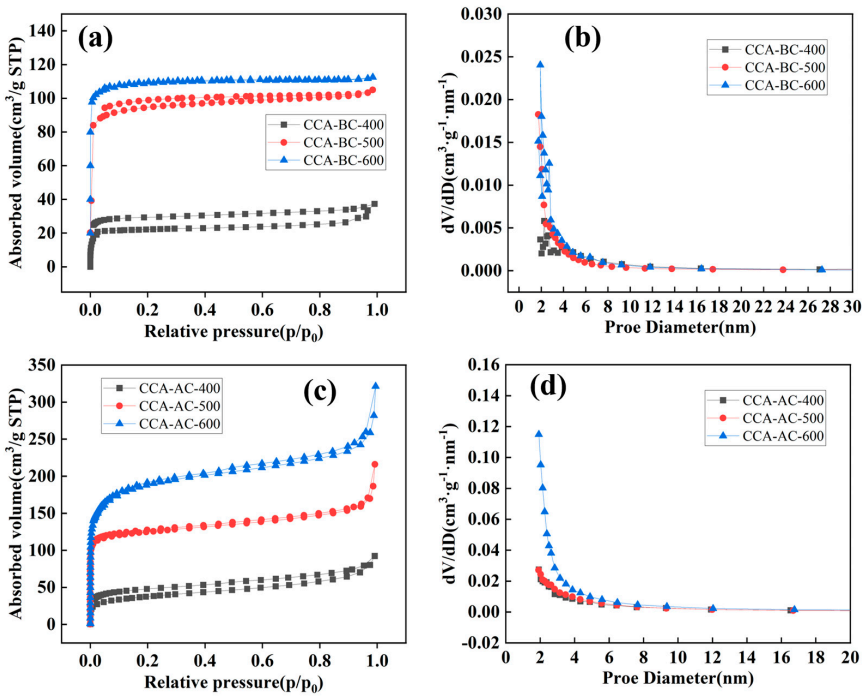

Figure 5. N_2 adsorption/desorption curves and pore distributions of (**a**,**b**) CCA-BC samples, (**c**,**d**) CCA-AC samples.

Table 1. Detailed values of surface area, pore size and average pore volume of the samples.

Samples	Surface Area (m^2/g)	Pore Size (nm)	Average Pore Volume (cm^3/g)
CCA-BC-400	99.85	2.463	0.0575
CCA-BC-500	311.34	2.752	0.1825
CCA-BC-600	444.85	1.710	0.1978
CCA-AC-400	191.10	4.290	0.1413
CCA-AC-500	570.18	2.651	0.3191
CCA-AC-600	884.62	2.638	0.4503

3.3. The Electrochemical Properties of the Biochar Samples

Electrochemical experiments were subsequently conducted on the CCA-BC-x and CCA-AC-x samples to examine their potential as supercapacitance electrodes. Figure 6a,b illustrates the volt–ampere characteristic (CV) curves of CCA-AC and CCA-BC samples scanned at 80 mV/s. The specific capacitance values of these samples were also listed in Table 2 compared with their corresponding W-AC and W-BC samples (Figure S7a,b); the CCA treated wood derived biochar samples provided higher CV area, indicating that the existence of metal compounds could remarkably enhance the energy storage capability of the biochar sample. Meanwhile, it was also illustrated that all CCA-AC and CCA-BC samples exhibited a quasi-rectangular loop in their CV curves in which a non-obvious redox peak was observed, which revealed their quick electrochemical response with electrical double layer capacitance behavior [21,45]. The reality is different from what we would ideally like due to relatively low amounts of incorporation of the metal compounds in the biochar (~3 wt% from XPS results). Moreover, all CCA-AC-x samples exhibited higher specific capacitance values than their corresponding CCA-BC-x samples, manifesting that the chemical activation treatment could facilitate the storage and transfer of charges due to the generation of more abundant hierarchical pore structures and functional groups. Specifically, both CCA-AC and CCA-BC obtained at 600 °C had the highest specific capacitance compared with the samples obtained at lower pyrolysis temperatures, which indicated that a higher pyrolysis temperature was beneficial for the establishment of charge transfer pathways. The CCA-AC-600 CV curves at various scan rates (Figure S7c) showed that there was no discernible distortion in the enclosed area as the scan rate rose. This indicates that carbon electrodes have a high-quality and fast scanning speed capacitance when the electrode–electrolyte ion interaction is restricted [25].

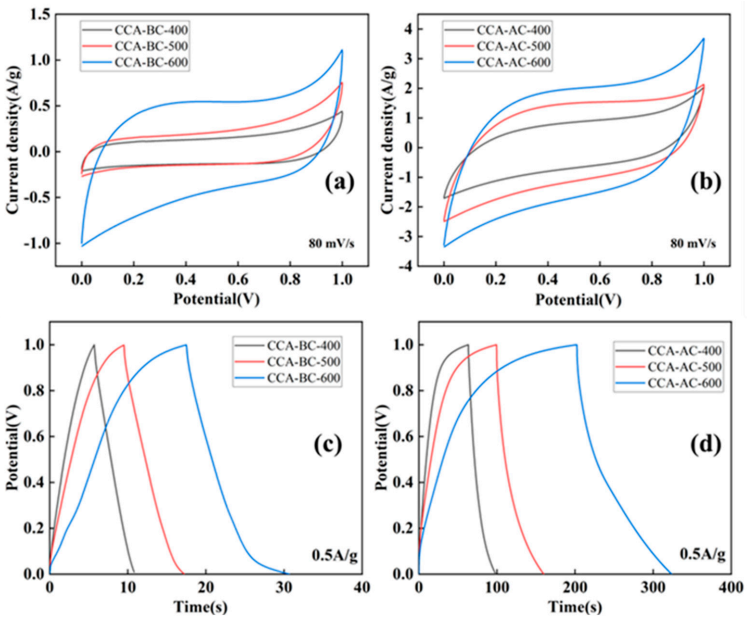

Figure 6. CV curves and GCD curves of (**a**,**c**) CCA-BC samples, (**b**,**d**) CCA-AC samples.

Table 2. The specific capacitance calculated from the CV and GCD curves.

Sample	Specific Capacitance (CV) (F/g)	Specific Capacitance (GCD) (F/g)
CCA-BC-400	3.91	2.57
CCA-BC-500	11.91	3.91
CCA-BC-600	5.13	6.60
CCA-AC-400	14.26	17.91
CCA-AC-500	22.23	58.98
CCA-AC-600	32.69	76.66
W-BC-500	4.34	5.16
W-AC-500	6.53	8.25

GCD testing was used to further examine the electrochemical characteristics of the produced biochar electrodes; the findings are displayed in Figure 6c,d. Two charge–discharge plateaus were visible in the electrode GCD curves of the BC sample. Excellent redox reversibility between the electrolyte and electrodes was indicated by two electrodes that displayed almost symmetric charge and discharge curves [39]. Nonetheless, for the electrode of the AC samples, the charged capacitance is greater than the corresponding discharged value, most likely as a result of the electrolyte ions' irreversible adsorption or redox reaction onto the more resistant amorphous carbon matrix [46]. Additionally, some kind of distortions was also observed from all curves due to the presence of metal compounds which generated pseudocapacitance behaviors. As anticipated, the CCA-AC and CCA-BC samples also exhibited better performance than their corresponding W-AC and W-BC electrodes (Figure S7c,d). In the meantime, CCA-AC samples had longer charge/discharge times than their CCA-BC samples, indicating that the electrodes made of activated biochar had a higher capacity for storing charge, which was in line with the findings of the CV test. The GCD results showed that the CCA-AC-600 had the highest specific capacitance values (Table 2), calculated at 76.7 F/g at 0.5 A/g. Additionally, when the current density was raised from 0.2 A/g to 1 A/g, CCA-AC-600 only lost 30% of its initial specific capacitance, indicating its promising charge/discharge stability. Compared with many reported wood derived biochar electrodes [47,48], CCA-AC-600 also exhibited a more remarkable electrochemical performance.

Figure 7 shows the Nyquist impedance plots for the CCA-BC and CCA-AC samples, which revealed the ohmic resistance of the biochar-based electrodes. The Nyquist diagram typically consists of a straight-line component in the region of low frequencies that represents the internal resistance of the circuit and electrolyte, and a semicircle with a straight line in the high-frequency zone that comprises a diameter reflecting the charge-transfer reluctance [49]. Figure 7 showed that all sample resistances were less than 4 Ω and that, as the pyrolysis temperature increased, the semicircle diameters of the CCA-BC and CCA-AC electrodes shrank. The results indicated that the biochar obtained at a higher pyrolysis temperature had a smaller resistance, which is in accordance with the above discussed results. Compared with the CCA-BC electrodes, all the corresponding CCA-AC electrodes presented a much smaller resistance semicircle and a more approximate vertical curve, which revealed their more remarkable capacitance performance. Figure 7c displays the findings of an investigation into the electrode's cyclic stability. As shown, under 2000 cycles of charge and discharge with a current density of 1 A/g, the CCA-AC-600-based electrode could still maintain 72% of its initial specific capacitance, which verified its promising cycling stability.

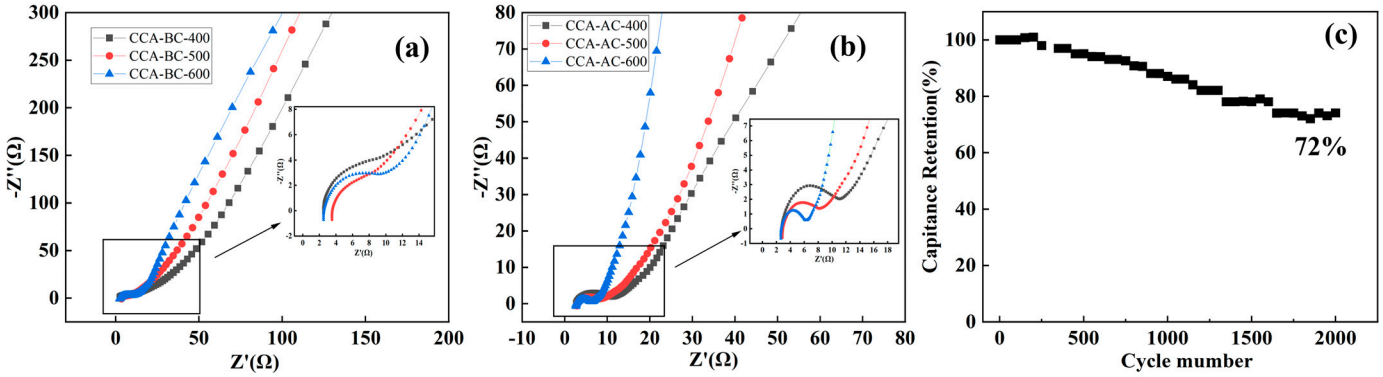

Figure 7. Nyquist EIS plots of (**a**) CCA-BC and (**b**) CCA-AC samples, (**c**) GCD cycle performance of CCA-AC-600.

4. Conclusions

To conclude, supercapacitor electrodes with excellent performance were prepared by pyrolyzing CCA-treated wood waste with KOH activation. The results showed that with the assistance of KOH activation, the CCA-AC showed both a large specific surface area and a porous structure arranged hierarchically. Amongst all obtained biochar samples, the greatest properties were displayed by CCA-AC-600, which also had the largest specific capacitance of 76.7 F/g and the highest specific surface area of 885 m^2/g. Moreover, the CCA-AC-600-based electrode had a promising retention capacity of nearly 72% after 2000 cycles. Through exploring the potential application of CCA-treated wood waste derived from biochar as the supercapacitance electrode, this study provides a new approach to convert wood waste into a high-value-added product.

Supplementary Materials: The following supporting information can be downloaded at https://www.mdpi.com/article/10.3390/f15010177/s1, Text S1: Chemicals and reagents. Text S2: Calculation of specific capacitance of the samples by CV curves. Text S3: Calculation of specific capacitance of the samples by GCD curves. Figure S1: A picture of CCA-treated wood and A SEM image of CCA-BC-600 with pits. Figure S2: EDS elemental mapping of (a) Cu, (b) Cr, (c) As in the powder of preservative wood. Figure S3: EDS elemental mapping of (a) O, (b) C, (c) Cu, (d) Cr, (e) As, and (f) K in CCA-AC-600. Figure S4: XRD spectra of W-BC-500 and W-AC-500. Figure S5: XPS spectra of W-BC-500, W-AC-500. Figure S6: XPS O1s spectra of (a) CCA-BC-600 and (b) CCA-AC-600. Figure S7: (a) CV curves and (b) GCD curves of W-BC-500 W-AC-600, (c) CV curves of CCA-AC-600 at different scan rate and (d) GCD curves of CCA-AC-600 at current density. Table S1: The ID/IG ratio determined from the Raman spectrum. Table S2: Elemental proportion from XPS analysis.

Author Contributions: The experiments were designed and the manuscripts were written by M.H. and J.S. The experiments were carried out by M.H., B.D. and J.L., who also discussed the outcomes. The manuscript was revised by J.S. and C.X. All authors have read and agreed to the published version of the manuscript.

Funding: This study was funded by Qing Lan Project of Jiangsu Province (2022).

Data Availability Statement: The data in this study can be obtained from the corresponding author.

Acknowledgments: Nanjing Forestry University Modern Analysis and Testing Center is acknowledged for providing the use of the related facilities.

Conflicts of Interest: There is no conflict of interest declared by the authors.

References

1. De Medeiros Domingos, D.; Scussel, R.; Canever, S.B.; Soares, B.Q.; Angioletto, E.; Bernardin, A.M.; Pich, C.T. Toxicity of fly ash effluent from the combustion of (chromated copper arsenate)-treated wood. *Clean. Mater.* **2022**, *3*, 100051. [CrossRef]
2. Chen, A.Y.; Olsen, T. Chromated copper arsenate–treated wood: A potential source of arsenic exposure and toxicity in dermatology. *Int. J. Women's Dermatol.* **2016**, *2*, 28–30. [CrossRef] [PubMed]

3. Wasson, S.J.; Linak, W.P.; Gullett, B.K.; King, C.J.; Touati, A.; Huggins, F.E.; Chen, Y.; Shah, N.; Huffman, G.P. Emissions of chromium, copper, arsenic, and PCDDs/Fs from open burning of CCA-treated wood. *Environ. Sci. Technol.* **2005**, *39*, 8865–8876. [CrossRef] [PubMed]
4. Ai, C.; Mccarthy, S.; Liang, Y.; Rudrappa, D.; Qiu, G.; Blum, P. Evolution of copper arsenate resistance for enhanced enargite bioleaching using the extreme thermoacidophile metallosphaera sedula. *J. Ind. Microbiol. Biotechnol.* **2017**, *44*, 1613–1625. [CrossRef]
5. Morais, S.; Fonseca, H.M.A.C.; Oliveira, S.M.R.; Oliveira, H.; Gupta, V.K.; Sharma, B.; de Lourdes Pereira, M. Environmental and health hazards of chromated copper arsenate-treated wood: A review. *Int. J. Environ. Res. Public Health* **2021**, *18*, 5518. [CrossRef]
6. Mercer, T.G.; Frostick, L.E. Evaluating the potential for environmental pollution from chromated copper arsenate (CCA)-treated wood waste: A new mass balance approach. *J. Hazard. Mater.* **2014**, *276*, 10–18. [CrossRef]
7. Gress, J.; Da Silva, E.B.; de Oliveira, L.M.; Zhao, D.; Anderson, G.; Heard, D.; Stuchal, L.D.; Ma, L.Q. Potential arsenic exposures in 25 species of zoo animals living in CCA-wood enclosures. *Sci. Total Environ.* **2016**, *551–552*, 614–621. [CrossRef]
8. EPA. Chromated Arsenicals (CCA). 2022. Available online: https://www.epa.gov/ingredients-used-pesticide-products/chromated-arsenicals-cca (accessed on 28 September 2023).
9. Maietta, M.; Colombo, R.; Lavecchia, R.; Sorrenti, M.; Zuorro, A.; Papetti, A. Artichoke (*Cynara cardunculus* L. var. *scolymus*) waste as a natural source of carbonyl trapping and antiglycative agents. *Food Res. Int.* **2017**, *100*, 780–790. [CrossRef]
10. Gigar, F.Z.; Khennane, A.; Liow, J.; Tekle, B.H.; Katoozi, E. Recycling timber waste into geopolymer cement bonded wood composites. *Constr. Build. Mater.* **2023**, *400*, 132793. [CrossRef]
11. Nelson, J.; Pickering, K.L.; Beg, M.D.H. Assessment of the potential of waste copper chromium and arsenic (CCA)-treated timber fibre reinforced polypropylene composites for construction. *J. Compos. Sci.* **2023**, *7*, 48. [CrossRef]
12. Xing, D.; Koubaa, A.; Tao, Y.; Magdouli, S.; Li, P.; Bouafif, H.; Zhang, J. Copper-doped carbon nanodots with superior photocatalysis, directly obtained from chromium-copper-arsenic-treated wood waste. *Polymers* **2023**, *15*, 136. [CrossRef]
13. Chen, Y.; Hou, H.; Liu, B.; Li, M.; Chen, L.; Chen, C.; Wang, S.; Li, Y.; Min, D. Wood-derived scaffolds decorating with nickel cobalt phosphate nanosheets and carbon nanotubes used as monolithic electrodes for assembling high-performance asymmetric supercapacitor. *Chem. Eng. J.* **2023**, *454*, 140453. [CrossRef]
14. Shan, L.; Zhang, Y.; Xu, Y.; Gao, M.; Xu, T.; Si, C. Wood-based hierarchical porous nitrogen-doped carbon/manganese dioxide composite electrode materials for high-rate supercapacitor. *Adv. Compos. Hybrid Mater.* **2023**, *6*, 174. [CrossRef]
15. Zhong, C.; Deng, Y.; Hu, W.; Qiao, J.; Zhang, L.; Zhang, J. A review of electrolyte materials and compositions for electrochemical supercapacitors. *Chem. Soc. Rev.* **2015**, *44*, 7484–7539. [CrossRef] [PubMed]
16. Liu, C.; Li, F.; Ma, L.; Cheng, H. Advanced materials for energy storage. *Adv. Mater.* **2010**, *22*, E28–E62. [CrossRef]
17. Chatterjee, D.P.; Nandi, A.K. A review on the recent advances in hybrid supercapacitors. *J. Mater. Chem. A* **2021**, *9*, 15880–15918. [CrossRef]
18. Wei, W.; Chen, Z.; Zhang, Y.; Chen, J.; Wan, L.; Du, C.; Xie, M.; Guo, X. Full-faradaic-active nitrogen species doping enables high-energy-density carbon-based supercapacitor. *J. Energy Chem.* **2020**, *48*, 277–284. [CrossRef]
19. Guo, Y.; Chen, C.; Wang, Y.; Hong, Y.; Wu, H.; Wang, K.; Niu, D.; Zhang, C.; Zhang, Q. Cu/Cu_xO@C nanocomposites as efficient electrodes for high-performance supercapacitor devices. *Dalton Trans.* **2022**, *51*, 14551–14556. [CrossRef] [PubMed]
20. Shinde, P.A.; Olabi, A.G.; Chodankar, N.R.; Patil, S.J.; Hwang, S.; Abdelkareem, M.A. Realizing superior redox kinetics of metal-metal carbides/carbon coordination supported heterointerface for stable solid-state hybrid supercapacitor. *Chem. Eng. J.* **2023**, *454*, 140246. [CrossRef]
21. Juni, F.J.; Majid, S.R.; Yusuf, S.N.F.; Osman, Z. Electrochemical characteristics of Cu/Cu_2O/C composite electrode for supercapacitor application. *Microchem. J.* **2021**, *164*, 106055. [CrossRef]
22. He, X.; Hu, Y.; Tian, H.; Li, Z.; Huang, P.; Jiang, J.; Wang, C. In-situ growth of flexible 3D hollow tubular Cu_2S nanorods on Cu foam for high electrochemical performance supercapacitor. *J. Mater.* **2020**, *6*, 192–199. [CrossRef]
23. Malaie, K.; Ganjali, M.R.; Alizadeh, T.; Norouzi, P. Simple electrochemical preparation of nanoflake-like copper oxide on Cu-plated nickel foam for supercapacitor electrodes with high areal capacitance. *J. Mater. Sci. Mater. Electron.* **2017**, *28*, 14631–14637. [CrossRef]
24. Wang, H.; Yoshio, M.; Thapa, A.K.; Nakamura, H. From symmetric ac/ac to asymmetric ac/graphite, a progress in electrochemical capacitors. *J. Power Sources* **2007**, *169*, 375–380. [CrossRef]
25. Choudhury, A.; Kim, J.; Yang, K.; Yang, D. Facile synthesis of self-standing binder-free vanadium pentoxide-carbon nanofiber composites for high-performance supercapacitors. *Electrochim. Acta* **2016**, *213*, 400–407. [CrossRef]
26. Gan, L.; Geng, A.; Xu, L.; Chen, M.; Wang, L.; Liu, J.; Han, S.; Mei, C.; Zhong, Q. The fabrication of bio-renewable and recyclable cellulose based carbon microspheres incorporated by $CoFe_2O_4$ and the photocatalytic properties. *J. Clean. Prod.* **2018**, *196*, 594–603. [CrossRef]
27. Mödlinger, M.; Provino, A.; Solokha, P.; Caglieris, F.; Ceccardi, M.; Macciò, D.; Pani, M.; Bernini, C.; Cavallo, D.; Ciccioli, A.; et al. Cu_3As: Uncommon crystallographic features, low-temperature phase transitions, thermodynamic and physical properties. *Materials* **2023**, *16*, 2501. [CrossRef] [PubMed]
28. Bahari, A.; Anasari, A.; Rahmani, Z. Low temperature synthesis of La_2O_3 and CrO_2 by sol—Gel process. *J. Eng. Technol. Res.* **2011**, *3*, 203–208.
29. Zhang, X.; Sun, B.; Fan, X.; Liang, P.; Zhao, G.; Saikia, B.K.; Wei, X. Hierarchical porous carbon derived from coal and biomass for high performance supercapacitors. *Fuel* **2022**, *311*, 122552. [CrossRef]
30. Robertson, J.; Ferrari, A.C. Interpretation of raman spectra of disordered and amorphous carbon. *Phys. Rev. B* **2000**, *61*, 14095–14107.

31. Wang, T.; Hu, S.; Wu, D.; Zhao, W.; Yu, W.; Wang, M.; Xu, J.; Zhang, J. Boosting the capacity of biomass-based supercapacitors using carbon materials of wood derivatives and redox molecules from plants. *J. Mater. Chem. A* **2021**, *9*, 11839–11852. [CrossRef]
32. Keiluweit, M.; Nico, P.S.; Johnson, M.G.; Kleber, M. Dynamic molecular structure of plant biomass-derived black carbon (biochar). *Environ. Sci. Technol.* **2010**, *44*, 1247–1253. [CrossRef]
33. Wang, Q.; Yan, J.; Wang, Y.; Wei, T.; Zhang, M.; Jing, X.; Fan, Z. Three-dimensional flower-like and hierarchical porous carbon materials as high-rate performance electrodes for supercapacitors. *Carbon* **2014**, *67*, 119–127. [CrossRef]
34. Zhang, Z.; Xi, J.; Zhou, H.; Qiu, X. KOH etched graphite felt with improved wettability and activity for vanadium flow batteries. *Electrochim. Acta* **2016**, *218*, 15–23. [CrossRef]
35. Zhang, C.; Long, D.; Xing, B.; Qiao, W.; Zhang, R.; Zhan, L.; Liang, X.; Ling, L. The superior electrochemical performance of oxygen-rich activated carbons prepared from bituminous coal. *Electrochem. Commun.* **2008**, *10*, 1809–1811. [CrossRef]
36. Wang, D.; Geng, Z.; Li, B.; Zhang, C. High performance electrode materials for electric double-layer capacitors based on biomass-derived activated carbons. *Electrochim. Acta* **2015**, *173*, 377–384. [CrossRef]
37. Lu, W.; Xu, L.; Shen, X.; Meng, L.; Pan, Y.; Zhang, Y.; Han, J.; Mei, X.; Qiao, W.; Gan, L. Highly efficient activation of sulfite by p-type S-doped g-C_3N_4 under visible light for emerging contaminants degradation. *Chem. Eng. J.* **2023**, *472*, 144708. [CrossRef]
38. Lesiak, B.; Kövér, L.; Tóth, J.; Zemek, J.; Jiricek, P.; Kromka, A.; Rangam, N. C sp^2/sp^3 hybridisations in carbon nanomaterials—XPS and (X)AES study. *Appl. Surf. Sci.* **2018**, *452*, 223–231. [CrossRef]
39. Liu, L.; Li, W.; Xiong, Z.; Xia, D.; Yang, C.; Wang, W.; Sun, Y. Synergistic effect of iron and copper oxides on the formation of persistent chlorinated aromatics in iron ore sintering based on in situ XPS analysis. *J. Hazard. Mater.* **2019**, *366*, 202–209. [CrossRef]
40. Oginni, O.; Singh, K.; Oporto, G.; Dawson-Andoh, B.; Mcdonald, L.; Sabolsky, E. Influence of one-step and two-step KOH activation on activated carbon characteristics. *Bioresour. Technol. Rep.* **2019**, *7*, 100266. [CrossRef]
41. Lu, W.; Qi, L.; Dong, D.; Shen, X.; Xu, L.; Zhang, Y.; Mei, X.; Qiao, W.; Guo, X.; Pan, Y. A comparison study of photocatalytic performance of g-C_3N_4 prepared from different precursors for the activation of different peroxides. *Sep. Purif. Technol.* **2023**, *327*, 124904. [CrossRef]
42. Sun, R.; Wang, X.; Wang, X.; Tan, B. Three-dimensional crystalline covalent triazine frameworks via a polycondensation approach. *Angew. Chem. Int. Ed.* **2022**, *61*, e202117668. [CrossRef]
43. Herath, A.; Layne, C.A.; Perez, F.; Hassan, E.B.; Pittman, C.U.; Mlsna, T.E. KOH-activated high surface area douglas fir biochar for adsorbing aqueous cr(vi), pb(ii) and cd(ii). *Chemosphere* **2021**, *269*, 128409. [CrossRef]
44. Ding, M.; Bannuru, K.K.R.; Wang, Y.; Guo, L.; Baji, A.; Yang, H.Y. Free-standing electrodes derived from metal–organic frameworks/nanofibers hybrids for membrane capacitive deionization. *Adv. Mater. Technol.* **2018**, *3*, 1800135. [CrossRef]
45. Feng, L.; Ding, R.; Chen, Y.; Wang, J.; Xu, L. Zeolitic imidazolate framework-67 derived ultra-small cop particles incorporated into n-doped carbon nanofiber as efficient bifunctional catalysts for oxygen reaction. *J. Power Sources* **2020**, *452*, 227837. [CrossRef]
46. Wu, Y.; Xu, G.; Zhang, W.; Song, C.; Wang, L.; Fang, X.; Xu, L.; Han, S.; Cui, J.; Gan, L. Construction of zif@electrospun cellulose nanofiber derived n doped metallic cobalt embedded carbon nanofiber composite as binder-free supercapacitance electrode. *Carbohydr. Polym.* **2021**, *267*, 118166. [CrossRef]
47. Woodward, R.T.; Markoulidis, F.; De Luca, F.; Anthony, D.B.; Malko, D.; Mcdonald, T.O.; Shaffer, M.S.P.; Bismarck, A. Carbon foams from emulsion-templated reduced graphene oxide polymer composites: Electrodes for supercapacitor devices. *J. Mater. Chem. A* **2018**, *6*, 1840–1849. [CrossRef]
48. Jiang, J.; Zhang, L.; Wang, X.; Holm, N.; Rajagopalan, K.; Chen, F.; Ma, S. Highly ordered macroporous woody biochar with ultra-high carbon content as supercapacitor electrodes. *Electrochim. Acta* **2013**, *113*, 481–489. [CrossRef]
49. Ma, Y.; Yin, J.; Liang, H.; Yao, D.; Xia, Y.; Zuo, K.; Zeng, Y. A two step approach for making super capacitors from waste wood. *J. Clean. Prod.* **2021**, *279*, 123786. [CrossRef]